US of Nerve Entrapments in Osteofibrous Tunnels of the Upper and Lower Limbs[1]

Carlo Martinoli, MD • Stefano Bianchi, MD • Nicola Gandolfo, MD
Maura Valle, MD • Stefano Simonetti, MD • Lorenzo E. Derchi, MD

CME FEATURE

See accompanying test at http://www.rsna.org/education/rg_cme.html

LEARNING OBJECTIVES FOR TEST 5

After reading this article and taking the test, the reader will be able to:

- Describe the most common nerve entrapment syndromes.
- Correlate the clinical abnormalities with the nerve entrapments.
- Recognize the US features of these lesions.

The diagnosis of nerve entrapment at osteofibrous tunnels relies primarily on clinical and electrodiagnostic findings. Recently, the refinement of high-frequency broadband transducers with a range of 5–15 MHz, sophisticated focusing in the near field, and sensitive color and power Doppler technology have improved the ability to evaluate peripheral nerve entrapment in osteofibrous tunnels with ultrasonography (US). In the upper limb, osteofibrous tunnels amenable to US examination include the carpal tunnel for the median nerve and the cubital and Guyon tunnels for the ulnar nerve. In the lower limb, these tunnels include the fibular neck for the common peroneal nerve, the tarsal tunnel for the posterior tibial nerve, and the intermetatarsal spaces for the interdigital nerves. High-resolution US allows direct imaging of the involved nerves, as well as documentation of changes in nerve shape and echotexture that occur in compressive syndromes. A spectrum of extrinsic causes of entrapment, such as tenosynovitis, ganglia, soft-tissue tumors, bone and joint abnormalities, and anomalous muscles, can also be diagnosed with US. With continued experience, it is likely that this technique will be increasingly used to evaluate nerve entrapment syndromes.

Index terms: Extremities, US, 40.1298 • Nerves, peripheral, 40.82 • Nervous system, US, 40.1298

RadioGraphics 2000; 20:S199–S217

[1]From the Department of Radiology R, University of Genoa, Largo Rosanna Benzi 8, I-16132 Genoa, Italy (C.M., L.E.D.); the Division of Radiodiagnostics, Hôpital Cantonal Universitaire, Geneva, Switzerland (S.B.); the Radiology Service, Ospedale Santa Corona, Pietra Ligure, Italy (N.G.); the Istituto Giannina Gaslini, Genoa, Italy (M.V.); and the Division of Neurology, E.O. Ospedali Galliera, Genoa, Italy (S.S.). Recipient of a Certificate of Merit award for a scientific exhibit at the 1999 RSNA scientific assembly. Received February 7, 2000; revision requested March 16 and received May 4; accepted May 11. **Address correspondence to** C.M. (e-mail: *martinoli@zeus.newnetworks.it*).

See the commentary by Miller.

Introduction

Current ultrasonography (US) systems equipped with linear-array transducers in the 5–15-MHz range have enabled radiologists to visualize most nerves with high conspicuity, demonstrate their proper fascicular structure, recognize specific abnormalities, differentiate endoneural from extraneural tumors, and evaluate the extent of the lesion and the status of the involved nerve at follow-up (1–4).

In nerve compression syndromes, diagnostic evaluation is based on clinical examination and electrophysiologic testing, which indicate the level and severity of the lesion. However, these studies do not provide spatial information about the nerve or its surroundings, which could help determine the cause (5). Direct visualization of nerve abnormalities with imaging modalities may enhance the diagnosis and the surgical result by providing exact information about the nature of constricting findings, especially in cases with confusing clinical pictures or equivocal or contradictory results at functional studies. At most centers, magnetic resonance (MR) imaging continues to be the standard for evaluation of the peripheral nervous system because image acquisition is not operator dependent, as it is in US, and interpretation is intuitively easier. However, high-resolution US allows low-cost and noninvasive imaging, is quickly performed, and has specific advantages over MR imaging in this area, including the capability for higher resolution and the ability to explore long segments of nerve trunks in a single study and examine tissues in both the static and dynamic state.

This article presents the anatomic bases, clinical characteristics, and US appearances of the most common nerve entrapments that occur in osteofibrous tunnels amenable to US examination. In the upper limb, these tunnels include the carpal tunnel for the median nerve and the cubital and Guyon tunnels for the ulnar nerve. In the lower limb, they include the fibular neck for the common peroneal nerve, the tarsal tunnel for the posterior tibial nerve, and the intermetatarsal spaces for the interdigital nerves. For each osteofibrous tunnel, specific scanning techniques and miscellaneous abnormalities that can be detected with US are also addressed.

Entrapment Neuropathies

Osteofibrous tunnels are narrow anatomic passageways that redirect the course of nerves along with tendons and vessels across synovial joints. The floor of these tunnels consists of bone, whereas the roof is made of focal transverse thickenings of the deep fascia, the retinacula, which are anchored at both ends to osseous prominences to prevent dislocation of and traumatic damage to the structures contained in the tunnel during joint activity. In these tunnels, nerves are more vulnerable to compression or entrapment than at other points along their course (5). The nerve compression may be external or due to the presence of abnormal tissue within the confined space of the tunnel. Chronic irritation of or pressure damage to the nerve may cause interference with the intraneural microvasculature, including ischemia due to compression of the vasa nervorum, disruption of the blood-nerve barrier, and venous congestion, which may lead to epineurial edema and increased endoneural fluid pressure (5,6). In early stages, symptoms may be intermittent or even cease after exercise parallel with recovery of intraneural circulation and drainage of intraneural edema. As the disease progresses, the prolonged edema of the epineurium may turn into fibrotic changes, further contributing to chronic constriction of the nerve (6). Long-standing compression causes damage in the myelin sheath and axonal degeneration induced by fibrosis, with permanent loss of nerve function and atrophy of the enervated muscles (5).

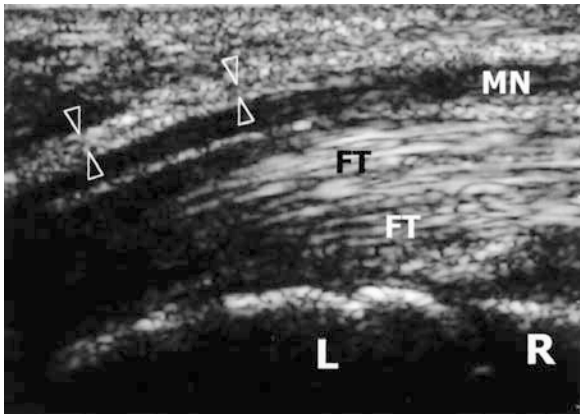

Figure 1. Carpal tunnel. Longitudinal 5–12-MHz US scan obtained in an asymptomatic 42-year-old man shows the hypoechoic median nerve (*MN*), which lies just underneath the flexor retinaculum (arrowheads) and superficial to the hyperechoic flexor tendons (*FT*). Note that the nerve angles away from the transducer on entering the tunnel. *L* = lunate, *R* = distal radius.

Carpal Tunnel

The median nerve enters the hand via a restricted passageway in the wrist, the carpal tunnel, which is delimited by the carpal bones and a roof consisting of the unextensible flexor retinaculum (transverse carpal ligament). Besides the median nerve, this tunnel contains eight tendons from the flexor digitorum superficialis and profundus and the tendon of the flexor pollicis longus (Fig 1). The retinaculum, which is approximately 3–4 cm wide, is attached to the tuberosity of the scaphoid and the

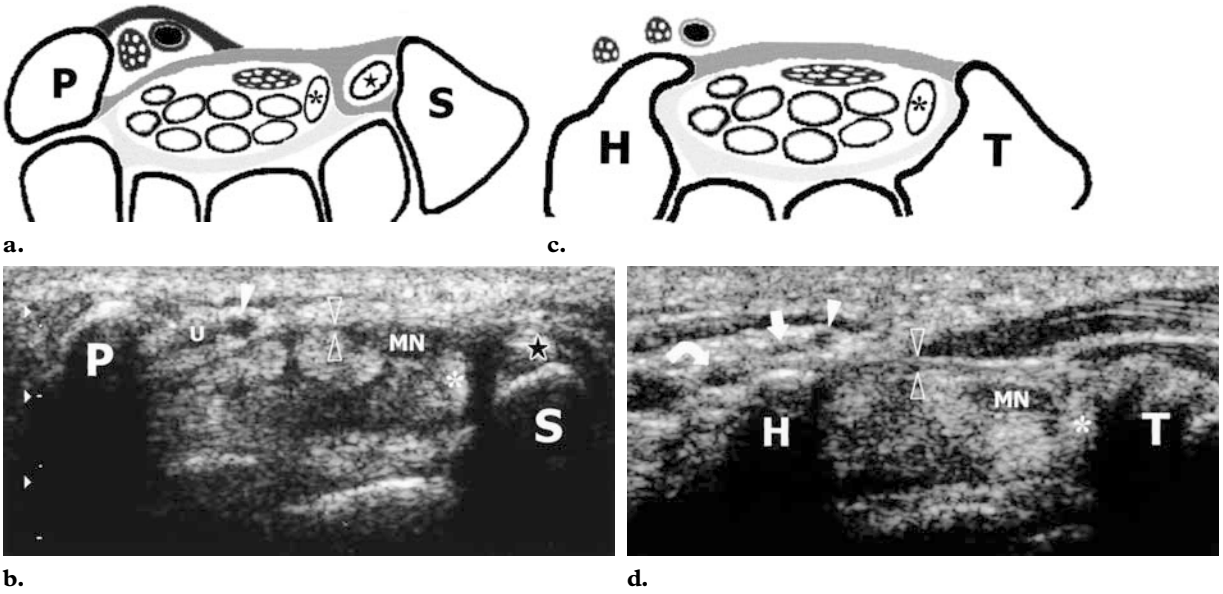

Figure 2. Carpal and Guyon tunnels. **(a, b)** Drawing **(a)** and corresponding transverse 5–12-MHz US scan **(b)** show the proximal level of the carpal tunnel delimited by the pisiform (*P*) and the scaphoid (*S*). **(c, d)** Drawing **(c)** and corresponding transverse 5–12-MHz US scan **(d)** show the distal level of the carpal tunnel delimited by the hook of the hamate (*H*) and the tubercle of the trapezium (*T*). The flexor retinaculum (medium gray region in **a** and **c**; open arrowheads in **b** and **d**) forms the roof of the carpal tunnel and the floor of the Guyon tunnel. The palmar carpal ligament (dark gray region in **a**) forms the volar boundary of the Guyon tunnel. The flexor tendons and median nerve (*MN*) extend through the carpal tunnel, with the nerve lying palmar and radial. At the level of the pisiform, the ulnar nerve (*U*) courses medial to the ulnar artery (solid arrowhead) within the Guyon tunnel. At the level of the hamate, the ulnar nerve divides into two terminal branches, a deep motor branch (curved arrow) and a superficial sensory branch (straight arrow). ∗ = flexor pollicis longus tendon, ★ = flexor carpi radialis tendon.

pisiform (proximal carpal tunnel) and to the tubercle of the trapezium and the hook of the hamate (distal carpal tunnel). On its radial side, it splits into two vertical layers to house the tendon of the flexor carpi radialis; then, it continues in the midportion of the palm as the palmar aponeurosis. The median nerve lies just under the retinaculum and courses superficial and parallel to the second and third flexor tendons and medial to the flexor pollicis longus tendon (Figs 1, 2). In the palm, it gives off sensory branches to the first, second, and third digits and the radial half of the fourth digit and a radial motor branch, which supplies the thenar muscles.

Compression of the median nerve at the carpal tunnel is the most common entrapment neuropathy. Symptoms include burning pain and paresthesia in the hand, which typically occur during sleep, and positive Tinel and Phalen signs (7). Sensory abnormalities are found in the median nerve distribution, whereas atrophy of the thenar eminence due to wasting of the abductor pollicis brevis, opponens pollicis, or flexor pollicis brevis muscle is considered a late sign of advanced neuropathy. The diagnosis of carpal tunnel syndrome is essentially based on the patient's history and clinical findings. Nerve conduction studies are usually not required but may be helpful to rule out proximal lesions of the nerve outside the carpal tunnel, including nerve root compression in the cervical spine and compression of the lower trunk of the brachial plexus at the thoracic outlet (5). Diagnostic imaging can be helpful in cases of carpal tunnel syndrome with unusual or atypical manifestations, for evaluation of suspected causes—especially to differentiate tenosynovitis of flexor tendons from other space-occupying lesions in the tunnel—and for assessment of postsurgical complications.

A wide spectrum of extrinsic causes of nerve entrapment may be recognized with US (8–11). These are related to congenital anomalies or acquired disease. Congenital anomalies include an aberrant flexor muscle of the index finger (Fig 3) and a persistent median artery of the forearm (Fig 4). Acquired disease can lead to increased content of the tunnel, as in tenosynovitis of flexor tendons (Fig 5), ganglion cyst, lipoma, vascular tumors (Fig 6), or amyloid deposits (Fig 7). Acquired

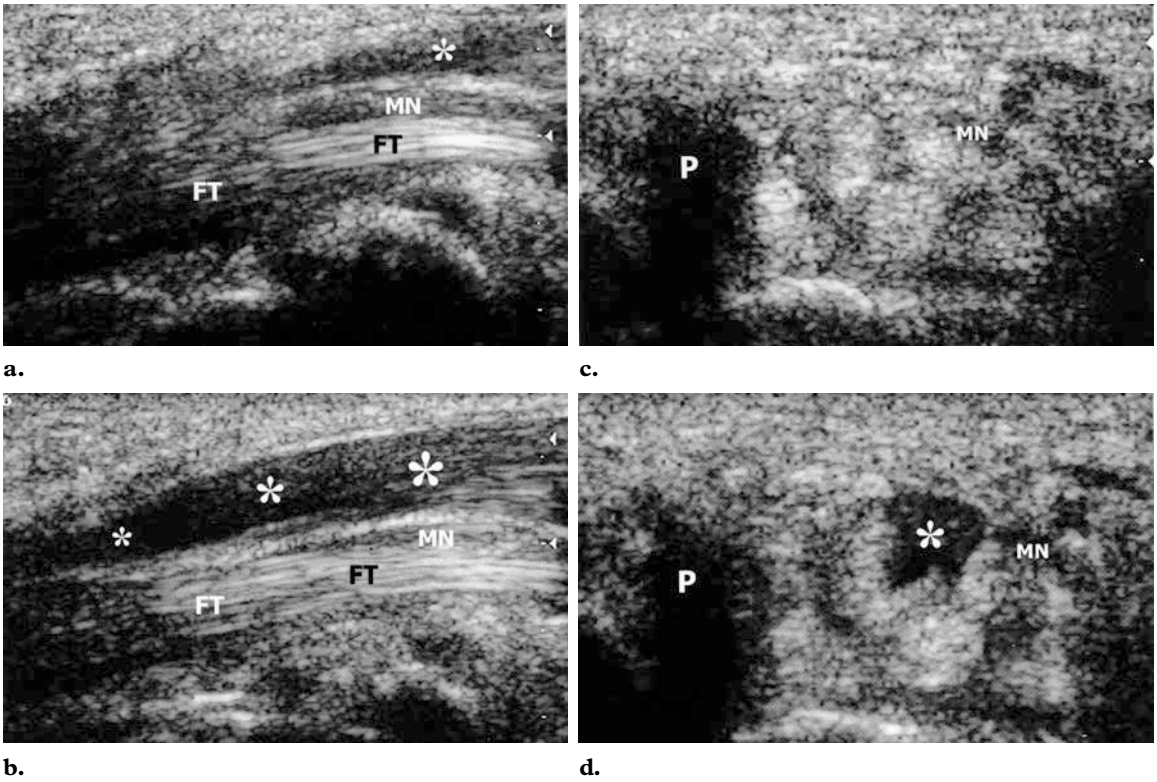

a. c.

b. d.

Figure 3. Carpal tunnel syndrome in a 65-year-old woman with an aberrant flexor muscle of the index finger. Longitudinal **(a, b)** and transverse **(c, d)** 5–12-MHz US scans of the carpal tunnel show the effects of flexion **(a, c)** and extension **(b, d)** of the index finger. With the fingers flexed, an anomalous muscle belly (∗) lies proximal to the entrance of the carpal tunnel. Progressive extension of the index finger pushes the muscle inside the tunnel, thus causing compression of the median nerve (*MN*). Flexion and extension of the other digits did not affect the position of this muscle. *FT* = flexor tendon, *P* = pisiform.

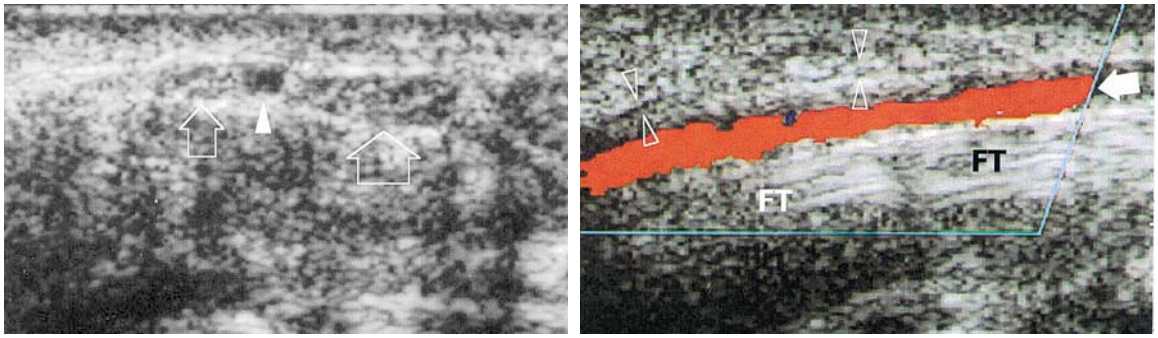

a. b.

Figure 4. Carpal tunnel syndrome in a 37-year-old man with a persistent median artery of the forearm. **(a)** Transverse 5–12-MHz gray-scale US scan obtained at the distal radius shows the proximal bifurcation of the median nerve (arrows) and the median artery of the forearm (arrowhead) located between the two nerve branches. **(b)** Longitudinal color Doppler US scan shows the course of the anomalous artery (arrow) through the carpal tunnel, superficial to the flexor tendons (*FT*) and deep to the flexor retinaculum (arrowheads). The presence of the artery causes disturbances in nerve function.

Figure 6. Carpal tunnel syndrome in a 40-year-old woman with a large intramuscular hemangioma extending through the flexor muscles of the forearm down to the carpal tunnel. The patient underwent release of the retinaculum 6 months earlier. **(a, b)** Longitudinal **(a)** and transverse **(b)** 5–13-MHz color Doppler US scans of the proximal carpal tunnel show an enlarged median nerve (arrows) containing abnormal vessels. *FT* = flexor tendon. **(c)** Coronal T2-weighted MR image (repetition time msec/echo time msec = 2,000/72) of the forearm shows the hemangioma (arrowheads) as a large hyperintense lesion involving the ventral aspect of the forearm, as well as the carpal tunnel. **(d, e)** Axial T2-weighted **(d)** and fat-suppressed T2-weighted **(e)** MR images (1,920/72) of the wrist show increased signal intensity in the epineurium surrounding the fascicles of the median nerve (arrow). This appearance is due to the presence of abnormal vessels within the nerve substance. ▶

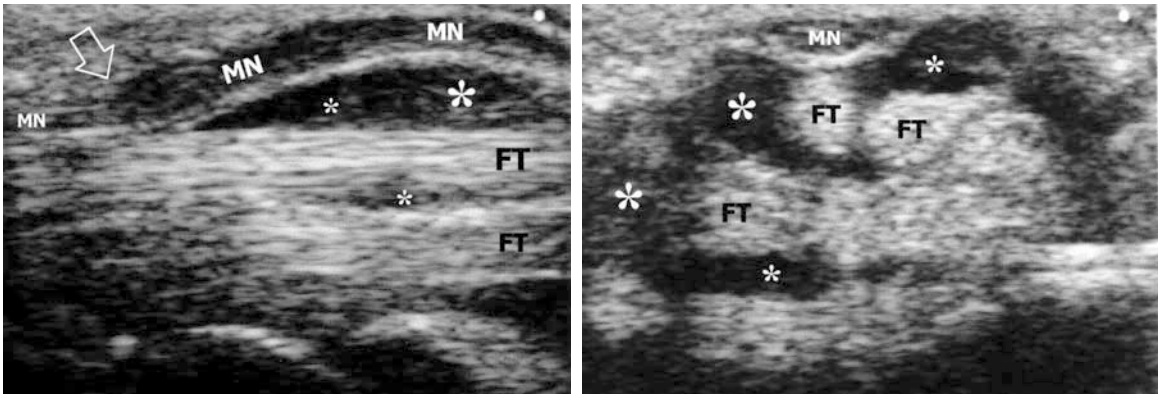

a. b.

Figure 5. Carpal tunnel syndrome in a 52-year-old man with rheumatoid arthritis. Longitudinal **(a)** and transverse **(b)** 10–13-MHz US images obtained at the distal radius show abnormally increased effusion (*) surrounding the flexor tendons (*FT*), resulting in palmar displacement and compression of the median nerve (*MN*) at the entrance to the tunnel (arrow).

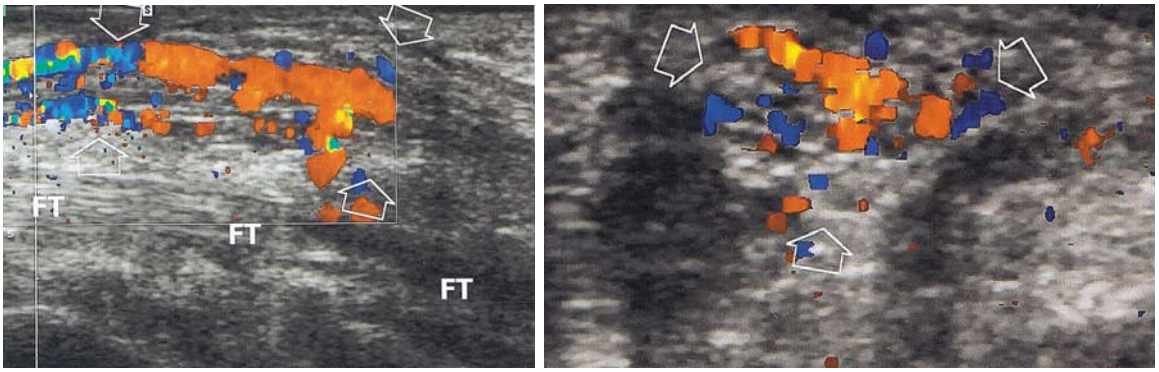

a. b.

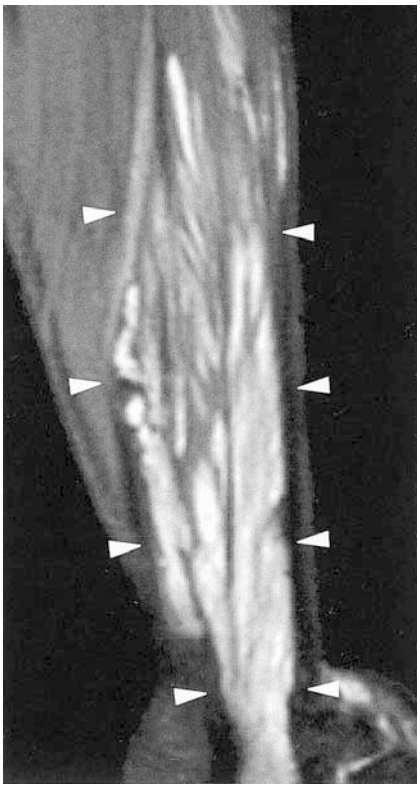

c.

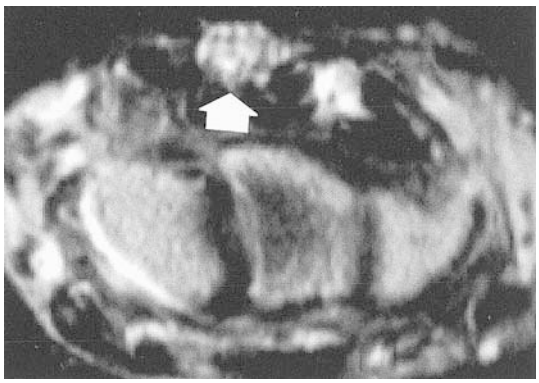

d.

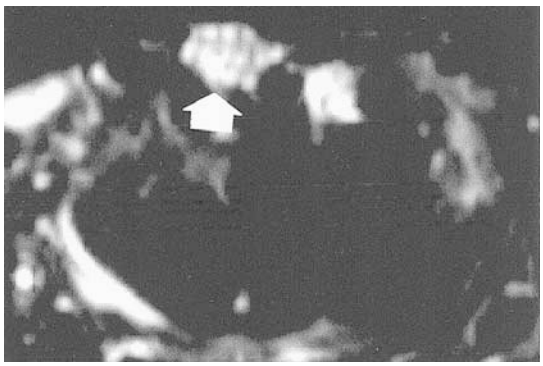

e.

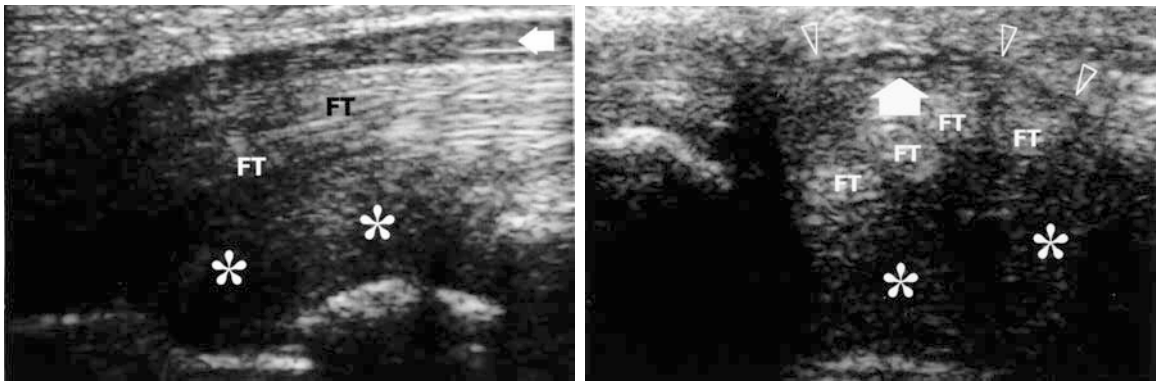

a. **b.**

Figure 7. Carpal tunnel syndrome in a 48-year-old woman with multiple myeloma and deposits of amyloid in the deep carpal tunnel. Longitudinal **(a)** and transverse **(b)** 5–12-MHz US scans show the bulk of the amyloid substance (∗) in the confined space of the tunnel, compressing the flexor tendons (*FT*) and median nerve (arrow) against the flexor retinaculum (arrowheads). Note the volar bulging of the retinaculum in **b**.

disease can also lead to decreased size of the tunnel, as in carpal bone malalignment (Fig 8) or bone fractures. In the surgical setting, US has been proposed as a guide for endoscopic release of the retinaculum (12,13).

During flexion of the fingers or fist clenching, longitudinal US scans demonstrate passive shifting of the median nerve along the underlying flexor tendons. On transverse US scans, the normal median nerve is elliptical and flattens progressively as it courses distally. US criteria for median nerve compression include the classic triad of nerve flattening in the distal tunnel, nerve swelling at the distal radius or (less frequently) in the proximal tunnel, and palmar bowing of the flexor retinaculum (8,14,15). Because the shape of the nerve varies as it passes through the tunnel, indexes have been introduced to better quantify abnormal findings; a nerve cross-sectional area greater than 0.09 cm^2 at the level of the proximal tunnel is reported to be the best criterion for the diagnosis (16). A good correlation has been demonstrated between the area of the median nerve measured with US and the severity of electromyographic findings or the functional outcome after surgery (17). Reduced transverse sliding of the nerve beneath the retinaculum during flexion and extension of the index finger may also be seen, but this sign is too subjective and harder to quantify (8,18). Only a few studies have compared US and MR imaging in evaluation of carpal tunnel syndrome. These studies demonstrated that US is capable of producing results at least equal to those of MR imaging (14). MR imaging appears to be superior to US in identification of subtle cases and has better sensitivity than color and power Doppler US in showing changes caused by nerve edema and blood perfusion abnormalities (19,20).

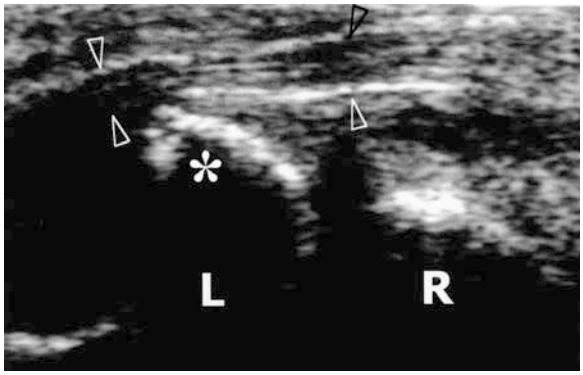

a.

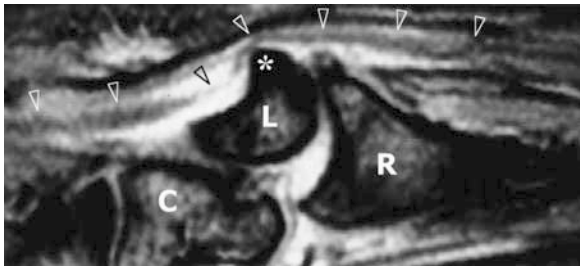

b.

Figure 8. Carpal tunnel syndrome in a 43-year-old man with perilunate dorsal dislocation of the wrist. Longitudinal 7.5–10-MHz US scan **(a)** and corresponding T2-weighted MR image (1,880/70) **(b)** of the carpal tunnel show the median nerve (arrowheads) compressed by a displaced lunate (*L*). Within the carpal tunnel, the lunate is prominent and has a crescentic profile. *C* = capitate, *R* = radius, ∗ = compression point.

After decompression, the appearance and mobility of the median nerve may improve, and it is possible to visualize the cleft in the retinaculum. Failure to improve after treatment is usually due to incomplete sectioning of the retinaculum (early complication) or scar tissue formation (late recurrence) (8).

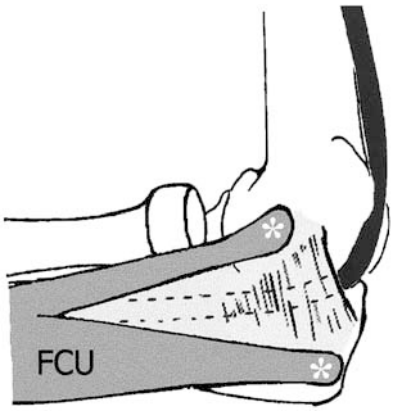

Figure 9. Cubital tunnel. **(a)** Drawing of the medial aspect of the elbow shows the course of the ulnar nerve (dark gray region) in the cubital tunnel. At the condylar groove, the nerve passes between the medial epicondyle and the olecranon, just deep to the cubital tunnel retinaculum and the arcuate ligament (light gray region) between the humeral and ulnar origins (*) of the flexor carpi ulnaris muscle (*FCU*). **(b, c)** Transverse 5–12-MHz US scans of the proximal tunnel **(b)** and distal tunnel **(c)** show the normal relationship of the ulnar nerve (arrow) to the medial epicondyle (*ME*) and the two heads of the flexor carpi ulnaris muscle (*). *O* = olecranon.

a.

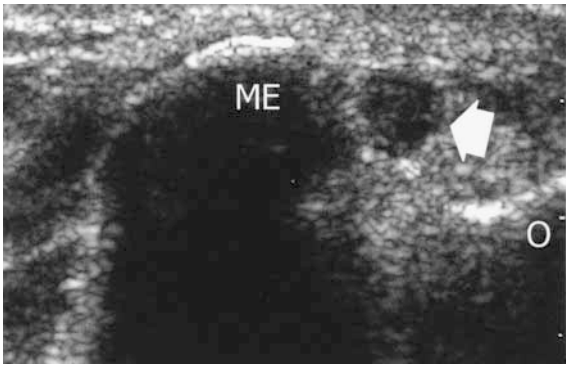

b.

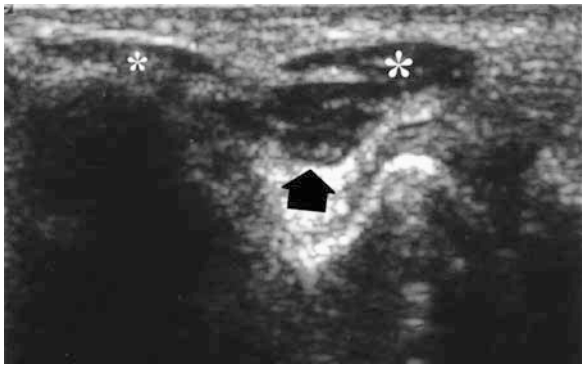

c.

Cubital Tunnel

In its passage around the medial aspect of the elbow, the ulnar nerve lies in an osteofibrous ring, the cubital tunnel, which is formed by a groove between the olecranon process of the ulna and the medial epicondyle of the humerus and bridged by a fascial sheet, the cubital tunnel retinaculum (also known as the Osborne fascia). Then, the nerve enters the hiatus between the ulnar and humeral heads of the flexor carpi ulnaris muscle; the origins of this muscle are connected by an aponeurotic arch, the arcuate ligament, which represents a distal expansion of the cubital tunnel retinaculum (Fig 9). In the cubital tunnel, the ulnar nerve is subcutaneous and may be palpable immediately posterior to the tip of the epicondyle. During elbow flexion and extension, the cubital tunnel changes in shape (from slightly ovoid to elliptical) and volume because of the eccentric origin of the retinaculum. As the ulnar nerve curves over the medial epicondyle, traction-related flattening and elongation of the nerve normally occur as the elbow flexes; in addition, an up to 55% decrease in cross-sectional area and a sixfold increase in interstitial pressure occur in the cubital tunnel as a result of increasing tension of the retinaculum and bulging of the medial collateral ligament (21). These factors may predispose the nerve to extrinsic compression at this level.

Lesions of the ulnar nerve typically manifest as medial elbow pain and a spectrum of symptoms ranging from sensory problems in the fourth and fifth fingers to motor problems in the muscles supplied by the nerve (flexor carpi ulnaris, flexor digitorum profundus of the fourth and fifth digits, hypothenar muscles, interosseous muscles of the hand). However, diagnosis with clinical examination and electromyography can be difficult because the ulnar nerve can be involved anywhere in the upper extremity (5). Pathologic conditions involving the cervical spinal roots and the brachial plexus may also mimic an ulnar neuropathy. Therefore, the entire course of the ulnar nerve should always be examined for abnormal structures that could be compressing it.

US evaluation of the cubital tunnel is best performed with small-field-of-view transducers to obtain full probe contact on the curvilinear osseous surfaces of the elbow joint. With larger transducers, thin, flexible standoff pads may facilitate scanning. If a pad is not available, a thick layer of gel and minimal probe pressure can be used instead. The patient is examined while supine with the arm abducted. Systematic scanning in transverse planes is preferred to follow the nerve. With longitudinal scans, the nerve may be easily confused with echoes

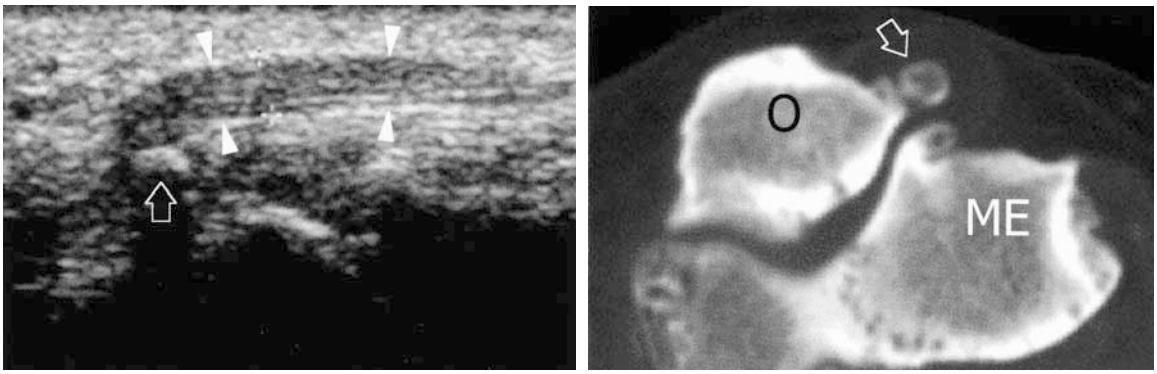

a. **b.**

Figure 10. Cubital tunnel syndrome in a 65-year-old man with a history of trauma to the elbow and heterotopic ossification in the cubital tunnel area. Longitudinal 7.5–10-MHz US scan **(a)** and axial computed tomographic (CT) scan **(b)** show an ossicle (arrow), which causes compression and reactive enlargement of the ulnar nerve (arrowheads) within the cubital tunnel. *ME* = medial epicondyle, *O* = olecranon.

from the triceps and flexor carpi ulnaris muscles, which course along the same plane. The ulnar nerve is identified throughout the cubital tunnel as an ovoid or bifid structure located close to the hyperechoic osseous cortex of the epicondyle (Fig 9). Owing to its curvilinear course, the nerve tends to appear less echogenic at the elbow than elsewhere in the upper limb as a result of anisotropy. Color Doppler imaging can help differentiate the nerve from the adjacent ulnar recurrent artery and veins. Unlike the thick retinaculum of the carpal tunnel, the cubital tunnel retinaculum consists of thin fascia and, at least in normal states, is not visualized.

Any swelling within the canal or inflammation and thickening of the fascial sheet may compress the nerve and its vasculature. There are two closely adjacent sites where the ulnar nerve may be compressed: one proximal, at the condylar groove; the other distal, at the edge of the aponeurosis of the flexor carpi ulnaris (5). In general, bone spurs in the condylar groove, heterotopic ossification in the cubital tunnel area (Fig 10), thickening of the medial collateral ligament on the floor of the tunnel, the anomalous anconeus epitrochlearis muscle, intraarticular loose bodies, ganglion cysts, or deformities from previous elbow fractures (cubitus valgus) may result in ulnar nerve entrapment (22,23). High-resolution US demonstrates abrupt narrowing and displacement of the nerve within the tunnel (Fig 11), often in association with abnormalities of adjacent structures. Occasionally, a thickened retinaculum can be observed at the level of compression. Proximal to this level, the nerve may appear swollen with loss of the fascicular pattern. At quantitative analysis with US, the cross-sectional area of the nerve at the epicondyle is significantly larger than in healthy subjects and significantly larger than the cross-sectional area of the normal contralateral nerve (24). After surgical decompression or translocation, US allows identification of scarring along the course of the nerve in patients with recurrent symptoms.

Guyon Tunnel

After descending the forearm between the flexor digitorum profundus and flexor carpi ulnaris muscles, the ulnar nerve pierces the deep fascia and enters the wrist through the Guyon tunnel. The walls of this canal consist of the pisiform medially and the hook of the hamate laterally; the floor is formed by the flexor retinaculum, and the roof is formed by the palmar carpal ligament and the palmaris brevis muscle (Fig 2). The Guyon tunnel houses the ulnar nerve, ulnar artery, and ulnar vein. In the distal canal, the ulnar nerve bifurcates into a superficial sensory branch and a deep motor branch, which supplies the hypothenar muscles and then passes across the palm, distributing to other intrinsic hand muscles. With transducers above 10 MHz in frequency, US is currently able to demonstrate the ulnar nerve at the pisiform level as a thin, rounded structure medial to the artery (Fig 2). The two terminal divisions of the nerve can also be visualized; the sensory branch continues to run in proximity to the ulnar artery, whereas the motor branch courses more deeply, adjacent to the medial surface of the hamate hook (Fig 2).

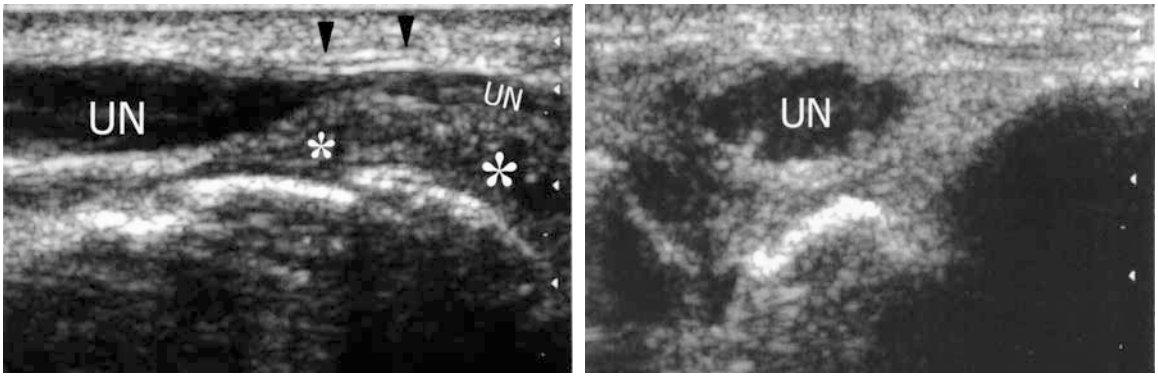

a. b.

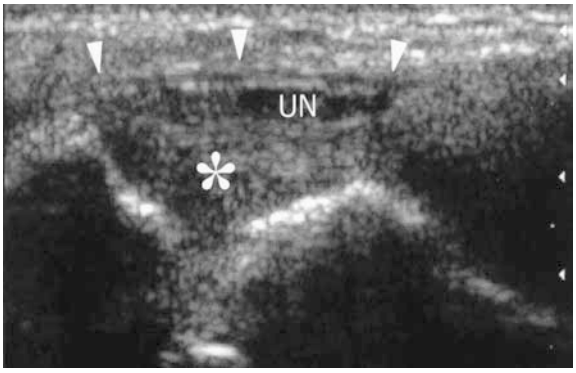

c.

Figure 11. Cubital tunnel syndrome in a 47-year-old woman with posttraumatic changes in the elbow resulting in cubitus valgus. Longitudinal 5–12-MHz US scan **(a)** and transverse 5–12-MHz US scans obtained at the distal arm **(b)** and within the cubital tunnel **(c)** show abrupt narrowing of the ulnar nerve (*UN*) between the thickened floor of the tunnel (*) and the retinaculum (arrowheads). Proximal to the tunnel, the nerve appears swollen and hypoechoic with an absent fascicular pattern.

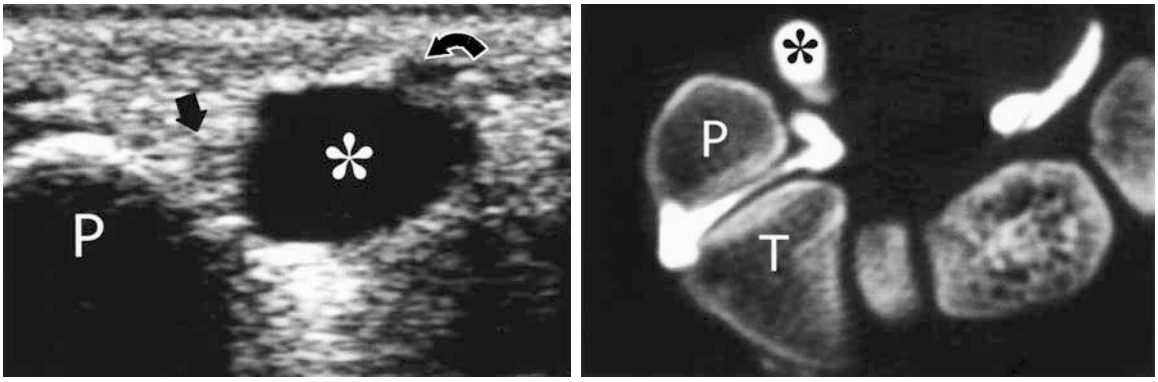

a. b.

Figure 12. Guyon tunnel syndrome in a 54-year-old man with a pisotriquetrum ganglion. Transverse 5–12-MHz US scan **(a)** and axial CT arthrogram **(b)** show a rounded, hypoechoic ganglion (*), which displaces the ulnar artery (curved arrow) and compresses the ulnar nerve (straight arrow) against the pisiform (*P*). *T* = triquetrum.

Ulnar neuropathies at the Guyon canal are rare; these include various syndromes according to the site of the lesion and the involvement of either the main nerve trunk or its divisions. Chronic repeated external pressure by tools, handles of canes, or crutches is the usual cause of nerve entrapment (5). On transverse scans, US allows detection of space-occupying lesions within the Guyon tunnel, such as ganglion cysts related to the pisotriquetrum joint space (Fig 12), anomalous muscles (accessory abductor digiti minimi, anomalous hypothenar adductor), pseudoaneurysms of the ulnar artery, and fracture residuals, which can cause compression of the nerve.

a.

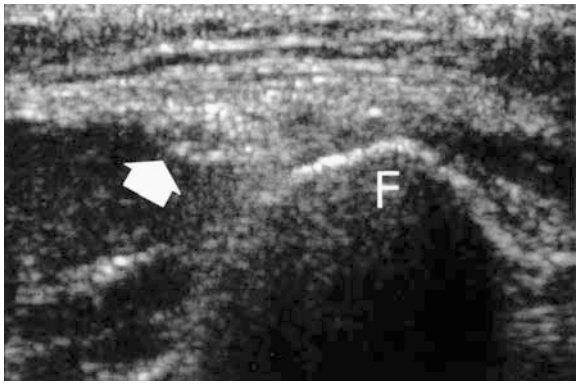

b.

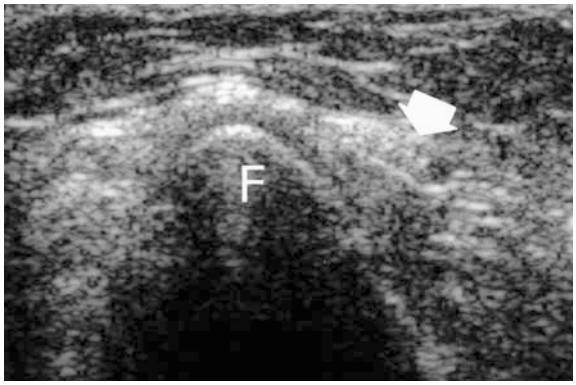

c.

Figure 13. Common peroneal nerve at the fibular neck. **(a)** Drawing of the anterolateral aspect of the leg shows the course of the common peroneal nerve (dark gray region) and its superficial and deep branches. The light gray region represents the insertion of the peroneus longus muscle. **(b, c)** Transverse 5–12-MHz US scans show the common peroneal nerve (arrow) before **(b)** and after **(c)** winding around the fibular neck. Note the close relationship of the nerve to the osseous surface of the fibula (*F*).

Fibular Neck

At the apex of the popliteal fossa, the sciatic nerve divides into two branches: the larger tibial nerve and the smaller common peroneal nerve. Whereas the tibial nerve continues the line of the sciatic nerve, the common peroneal nerve descends obliquely through the popliteal fossa to wind around the fibular neck. It passes deep to the attachment of the superficial head of the peroneus longus muscle and divides into two branches, the superficial and deep peroneal nerves, which have both sensory and motor fibers (Fig 13). The muscles supplied by the superficial peroneal nerve are evertors (peroneus longus and brevis) in the lateral compartment of the leg, whereas the deep peroneal nerve supplies the extensors and dorsiflexors of the foot and toes (tibialis anterior, extensor hallucis longus, extensor digitorum longus and brevis). A complete lesion of the common peroneal nerve leads to a characteristic footdrop and slapping gait, with sensory loss extended over the anterolateral surface of the lower leg and the dorsum of the foot.

Current US equipment with modern linear-array transducers in the 10–15-MHz frequency range is able to demonstrate the common peroneal nerve through the lateral portion of the popliteal fossa down to the fibular neck (Fig 13). The posterior margin of the biceps femoris tendon and the echogenic profile of the fibular head can be useful landmarks for identifying the nerve. Difficulties, if any, may arise in obese patients, in whom abundant subcutaneous fat can obscure the thin image of the nerve. Although relatively infrequent, entrapment of the common peroneal nerve typically occurs in the restricted space between the bone and the fascia as the nerve winds around the back of the fibular neck (25). In many instances, lesions probably result from pressure on the nerve at the fibular neck during sleep or from habitual leg crossing. However, nerve compression can also result from space-occupying lesions, including ganglion cysts, soft-tissue tumors, osseous masses, or a large fabella. Also, it may be secondary to a fracture, dislocation, application of skeletal traction, or a tight cast or bandage around the knee. Nerve sheath ganglia typically involve the common peroneal nerve by infolding in the space between the epineurium and the nerve fascicles. The origin of these ganglia has not yet been clarified, but many of them may be

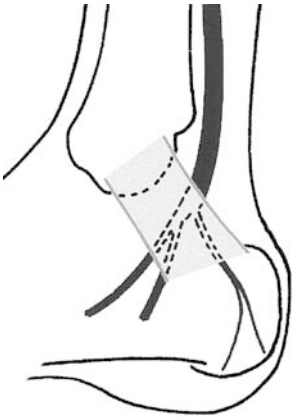

Figure 15. Tarsal tunnel. **(a)** Drawing of the medial aspect of the ankle shows the course of the tibial nerve (dark gray region) and its terminal branches, the medial and lateral plantar nerves and the calcaneal nerve, in the tarsal tunnel. Light gray region = flexor retinaculum tendon. **(b)** Transverse 5–12-MHz US scan of the retromalleolar region shows the retinaculum (arrowheads) and tibial nerve (arrow) close to the posterior tibial artery (*A*) and veins (*V*). *FDL* = flexor digitorum longus tendon. **(c)** Transverse 5–12-MHz US scan of the medial heel shows the medial and lateral plantar nerves (arrows) and calcaneal nerve (arrowhead). *A* = posterior tibial artery, *FHL* = flexor hallucis longus tendon, *V* = posterior tibial vein.

a.

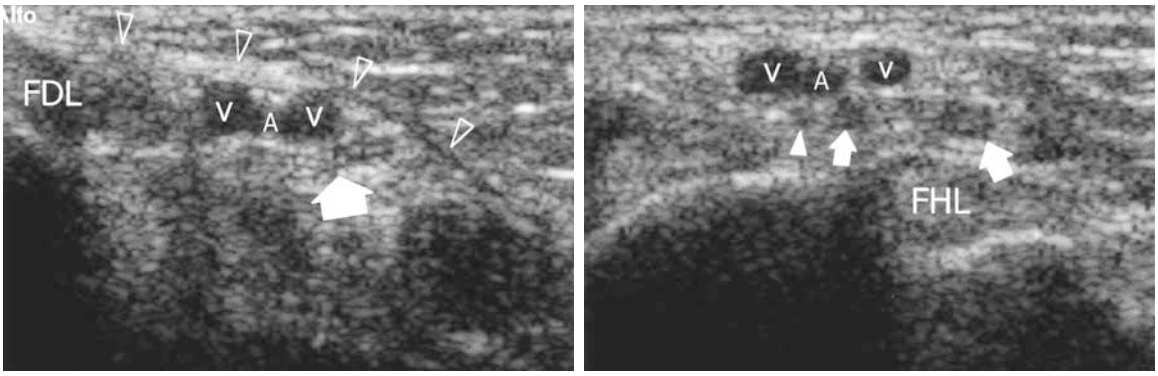

b. **c.**

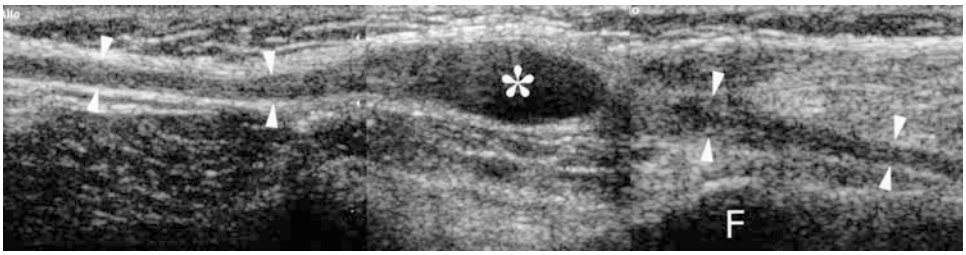

Figure 14. Common peroneal nerve entrapment by a ganglion in a 54-year-old man. Longitudinal 5–12-MHz US scan of the posterolateral knee shows a ganglion (*) that expands along the common peroneal nerve (arrowheads), thus leading to a compressive syndrome. The ganglion can be differentiated from the nerve substance on the basis of its cystic structure. *F* = fibula.

extensions of ganglia related to the tibiofibular joint with secondary nerve involvement, rather than primarily arising in the nerve sheath. US shows a spindle-shaped cystic structure within the nerve sheath (Fig 14). The hypoechoic cyst causes focal enlargement of the nerve bundle, and the entering and exiting nerve may be thickened with loss of fascicular structure, thus producing a tapering appearance of the cystic mass (4). Internal septations may be encountered.

Tarsal Tunnel

At the medial ankle, the tibial nerve, the continuation of the medial trunk of the sciatic nerve, passes deep to the flexor retinaculum in the interval between the medial malleolus and the medial wall of the calcaneus (Fig 15). The retinaculum consists of thin fascia and forms the roof of the tarsal tunnel. Along with the nerve, the tarsal tunnel encloses three tendons (tibialis posterior, flexor digitorum

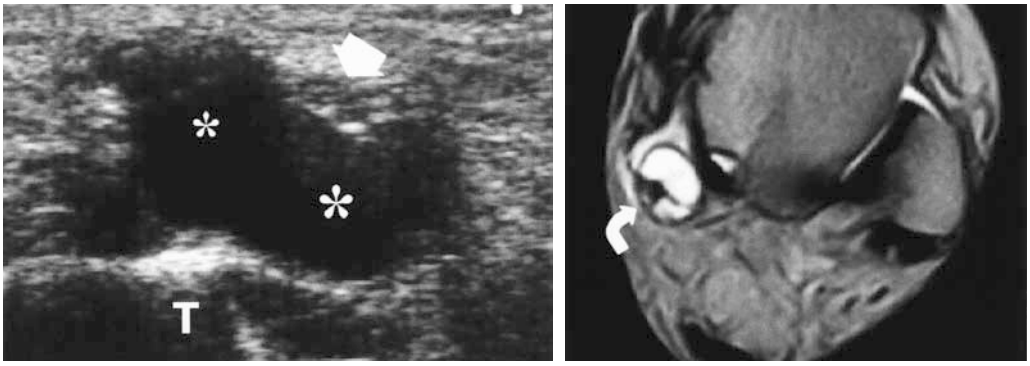

a. b.

Figure 16. Tarsal tunnel syndrome in a 61-year-old woman with a tibiotalar ganglion. Transverse 10–13-MHz US scan **(a)** and coronal T2-weighted MR image (2,000/80) **(b)** show a large ganglion (*) at the posteromedial ankle that displaces and expands around the tibial nerve (arrow), thus sustaining a compressive syndrome. *T* = talus.

Figure 17. Tarsal tunnel syndrome in a 32-year-old man with posttraumatic bone changes at the posteromedial ankle. **(a)** Longitudinal 10–13-MHz US scan shows focal fusiform thickening and a hypoechoic appearance of the tibial nerve (arrowheads) in the tarsal tunnel. **(b)** Transverse US scan obtained during eversion and dorsiflexion of the ankle shows anterior displacement of the tibial nerve (arrow) against a prominent bone (*). The nerve appears swollen and hypoechoic in comparison with its normal appearance (Fig 15b). *A* = posterior tibial artery, *V* = posterior tibial vein. **(c)** Axial CT scan shows a prominent bone spur (*) at the posteromedial aspect of the talus.

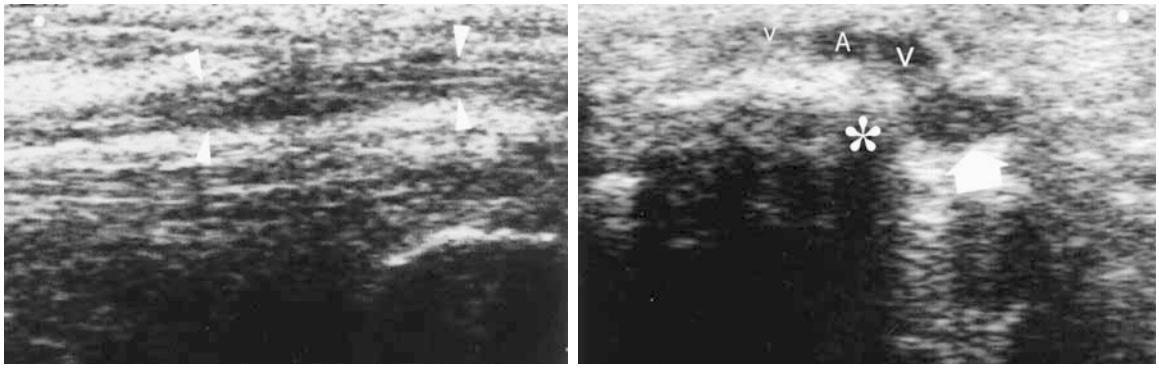

a. b.

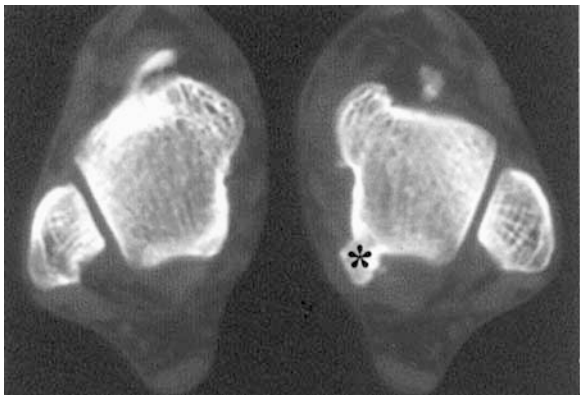

c.

longus, flexor hallucis longus), the posterior tibial artery, and the posterior tibial veins. Posteroinferior to the medial malleolus, the tibial nerve divides into the medial and lateral plantar nerves and a calcaneal sensory branch. The plantar nerves supply the intrinsic foot muscles, except for the extensor digitorum brevis, which is innervated by the deep peroneal nerve.

Proximal tarsal tunnel syndrome consists of entrapment of the tibial nerve in the retromalleolar region, whereas distal tarsal tunnel syndrome involves the divisions of the tibial nerve. In cases of standard tarsal tunnel syndrome, it should be assumed that the pathologic condition exists in both these zones; however, localized nerve disease involving only one of these nerves may occur (6). External compression resulting from ill-fitting footwear or tight plaster casts is probably the most common cause. However, space-occupying lesions of the medial ankle, such as flexor tenosynovitis, ganglia related to the talocalcaneal joint (Fig 16),

Figure 18. Morton neuroma. **(a)** Drawing of the forefoot shows the site of entrapment of the interdigital nerve (dark gray region) underneath the edge of the transverse intermetatarsal ligament (light gray region). **(b, c)** Transverse **(b)** and longitudinal **(c)** 5–12-MHz US scans, obtained with the transducer over the dorsal aspect of the metatarsal heads in a 44-year-old woman, show a Morton neuroma (arrow) between the second metatarsal (*II*) and third metatarsal (*III*). The lesion is hypoechoic and fusiform. The small interdigital nerve (arrowheads) is seen proximal to the mass. *IV* = fourth metatarsal.

a.

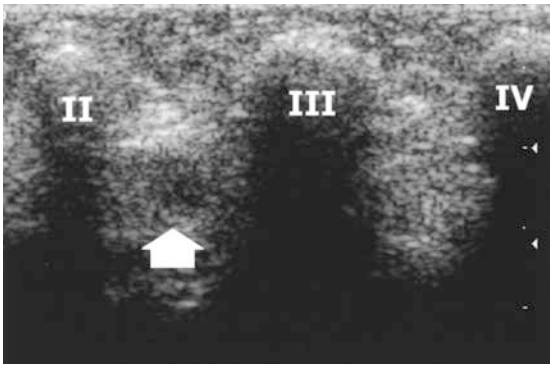

b.

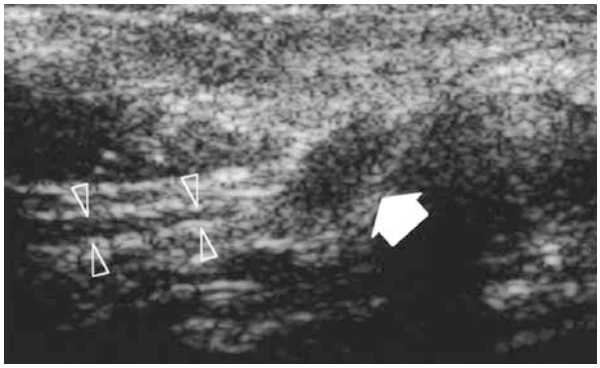

c.

fascial septa, an anomalous tendon or muscle (flexor digitorum accessorius longus), or fracture residuals (Fig 17), may also constrict the nerve (26). Although typical symptoms include numbness or pain in the foot and ankle and paresthesia in the sole of the foot, the clinical and electromyographic diagnosis of tarsal tunnel syndrome is often not straightforward, especially when a soft-tissue swelling on the medial ankle is absent.

With high-resolution transducers, US is able to demonstrate the complex anatomy of the tarsal tunnel and show the entire course of the tibial nerve and its branches at the medial ankle and medial heel (Fig 15). The tibial nerve lies posterior to the flexor digitorum longus tendon and superficial to the flexor hallucis longus tendon, close to the posterior tibial vessels. Identification of these vessels with color Doppler imaging may provide a useful landmark for visualizing the nerve. In cases of space-occupying lesions within the tunnel, US can provide exact information on the nature and extent of the constriction. Local fusiform thickening of the nerve, possibly associated with disappearance of the fascicular pattern, or a size discrepancy between the medial and lateral branches may also be demonstrated.

Intermetatarsal Spaces

The medial and lateral plantar nerves terminate near the bases of the metatarsals by dividing into interdigital nerves, which supply motor branches to the muscles of the sole and cutaneous branches to the digits. While proceeding toward the digits, the interdigital nerves pass deep to the transverse intermetatarsal ligament, which connects the metatarsal heads to maintain the transverse arch of the foot (Fig 18). Recurrent local impingement of the nerve underneath this ligament, with subsequent nerve structure degeneration and perineural fibrosis, is the most commonly accepted cause of Morton neuroma (interdigital neuritis) (27). Other possible causes include ischemia and compression of the interdigital nerve by an inflamed and enlarged intermetatarsal bursa (28). The main symptoms of Morton neuroma are pain in the forefoot with numbness and paresthesia in the adjacent toes. The symptoms are typically exacerbated by stressing of the metatarsal-phalangeal joints, as occurs with dorsiflexion of the toes or walking in narrow shoes. Although many orthopedic foot surgeons believe that Morton neuroma is diagnosed clinically, diagnostic imaging can help establish the

correct diagnosis and the location of the lesion, thus making the surgeon more confident about diagnostic and therapeutic decisions (29).

US evaluation can be performing by placing the probe on the dorsal (30,31) or plantar (32) aspect of the foot. For the dorsal approach, the toes are plantar flexed and manual pressure in the affected web space is applied on the plantar side. For the plantar approach, the toes are dorsiflexed and finger pressure is exerted in the web spaces on the dorsal side. Although the interdigital nerves run closer to the plantar surface of the foot, in our experience the quality of sonograms obtained by placing the probe on the dorsal surface is somewhat higher, probably due to the thinner skin and the absence of keratosis. However, both approaches can be performed in a patient to optimize visualization of the intermetatarsal spaces.

Owing to the relatively small size of normal interdigital nerves (approximately 2 mm in diameter), US examination of these nerves is problematic. Doppler imaging can aid in localization of the nerve by demonstrating the adjacent intermetatarsal artery and vein (33). Morton neuromas most frequently occur within the second or third interspace and are located at the level of or slightly proximal to the metatarsal heads. They appear as fusiform or ovoid hypoechoic masses elongated along the major axis of the metatarsals (30,32,34) (Fig 18). Beyond the tumor, the entering and exiting nerve may be slightly thickened and is therefore more easily identified than in normal subjects on longitudinal US scans. Power Doppler US may be helpful in identifying these lesions on the basis of their increased vascularity (35). Intense tenderness elicited by pressure with the transducer over the suspected neuroma supports the diagnosis. In the appropriate clinical setting, US has a reported sensitivity of 95%–100% (30,31,36) for detection of Morton neuromas, with a specificity of 83% and accuracy of 95% (31). Similar results have been reported for MR imaging, which has demonstrated a sensitivity of 87%, specificity of 100%, and accuracy of 89% (37). Small lesions (<5 mm in diameter) can be difficult to identify with US; this fact may explain the higher sensitivity of MR imaging in some series (31).

Conclusions

Although the application of US is limited by its inherent operator dependence and the relatively long learning curve needed to acquire this skill, this technique can be adequate and cost-effective for evaluating the involved nerve and adjacent processes that may be causing nerve compression in a variety of osteofibrous tunnels. In our opinion, US can be the first-line imaging technique in patients with suspected nerve entrapment syndromes and can obviate MR imaging in many cases. A careful US examination performed with an accurate, meticulous scanning technique and good knowledge of the anatomic relationships of nerves to surrounding structures may provide the clinician with precise information regarding the involved nerve and the site and nature of the disease process, facilitating selection of the appropriate treatment.

References

1. Fornage BD. Peripheral nerves of the extremities: imaging with US. Radiology 1988; 167: 179–182.
2. Graif M, Seton A, Nerubali J, et al. Sciatic nerve: sonographic evaluation and anatomic-pathologic considerations. Radiology 1991; 181:405–408.
3. Silvestri E, Martinoli C, Derchi LE, et al. Echotexture of peripheral nerves: correlation between US and histologic findings and criteria to differentiate tendons. Radiology 1995; 197: 291–296.
4. Martinoli C, Bianchi S, Derchi LE. Tendon and nerve sonography. Radiol Clin North Am 1999; 37:691–711.
5. Stewart JD. Compression and entrapment neuropathies. In: Dyck PJ, Thomas PK, eds. Peripheral neuropathy. 3rd ed. Philadelphia, Pa: Saunders, 1993; 1354–1379.
6. Shon LC. Nerve entrapment, neuropathy, and nerve dysfunction in athletes. Orthop Clin North Am 1994; 25:47–59.
7. Gelberman RH, Eaton R, Urbaniak JR. Peripheral nerve compression. J Bone Joint Surg Am 1993; 75:1854–1878.
8. Chen P, Maklad N, Redwine M, et al. Dynamic high-resolution sonography of the carpal tunnel. AJR Am J Roentgenol 1997; 168:533–537.
9. Bertolotto M, Rosenberg I, Parodi RC, et al. Fibroma of tendon sheath in the distal forearm with associated median nerve neuropathy: US, CT, and MR appearance. Clin Radiol 1996; 51: 370–372.
10. Van Vugt RM, van Dalen A, Bijlsma JW. The current role of high-resolution ultrasonography of the hand and wrist in rheumatic diseases. Clin Exp Rheumatol 1998; 16:454–458.
11. Kato H, Ogino T, Nanbu T, et al. Compression neuropathy of the motor branch of the median nerve caused by palmar ganglion. J Hand Surg [Am] 1991; 16:751–752.
12. Nakamichi K, Tachibana S. Distance between the median nerve and ulnar neurovascular bundle: clinical significance with ultrasonographically assisted carpal tunnel release. J Hand Surg [Am] 1998; 23:870–874.
13. Nakamichi K, Tachibana S. Ultrasonographically assisted carpal tunnel release. J Hand Surg [Am] 1997; 22:853–862.

14. Buchberger W, Schon G, Strasser K, et al. High-resolution ultrasonography of the carpal tunnel. J Ultrasound Med 1991; 10:531–537.
15. Buchberger W, Judmaier W, Birbamer G, et al. Carpal tunnel syndrome: diagnosis with high-resolution sonography. AJR Am J Roentgenol 1992; 159:793–798.
16. Duncan I, Sullivan P, Lomas F. Sonography in the diagnosis of carpal tunnel syndrome. AJR Am J Roentgenol 1999; 173:681–683.
17. Lee D, van Holsbeeck MT, Janevski PK, et al. Diagnosis of carpal tunnel syndrome: ultrasound versus electromyography. Radiol Clin North Am 1999; 37:859–872.
18. Nakamichi K, Tachibana S. Restricted motion of the median nerve in carpal tunnel syndrome. J Hand Surg [Br] 1995; 20:460–464.
19. Sugimoto H, Miyaji N, Ohsawa T. Carpal tunnel syndrome: evaluation of median nerve circulation with dynamic contrast-enhanced MR imaging. Radiology 1994; 190:459–466.
20. Martinoli C, Derchi LE, Bertolotto M, et al. US and MR imaging of peripheral nerves in leprosy. Skeletal Radiol 2000; 29:142–150.
21. Gelberman RH, Yamaguchi K, Hollstien SB, et al. Changes in interstitial pressure and cross-sectional area of the cubital tunnel and of the ulnar nerve with flexion of the elbow. J Bone Joint Surg Am 1998; 80:492–501.
22. O'Driscoll SW, Horii E, Carmichael SW, et al. The cubital tunnel and ulnar neuropathy. J Bone Joint Surg Br 1992; 74:84–94.
23. Puig S, Turkof E, Sedivy R, et al. Sonographic diagnosis of recurrent ulnar nerve compression by ganglion cysts. J Ultrasound Med 1999; 18: 433–436.
24. Chiou HJ, Chou YH, Cheng SP, et al. Cubital tunnel syndrome: diagnosis by high-resolution ultrasonography. J Ultrasound Med 1998; 17: 643–648.
25. Loredo R, Hodler J, Pedowitz R, et al. MRI of the common peroneal nerve: normal anatomy and evaluation of masses associated with nerve entrapment. J Comput Assist Tomogr 1998; 22: 925–931.
26. Nagaoka M, Satou K. Tarsal tunnel syndrome caused by ganglia. J Bone Joint Surg Br 1999; 81:607–610.
27. Alexander IJ, Johnson KA, Parr JW. Morton's neuroma: a review of recent concepts. Orthopedics 1987; 10:103–106.
28. Awerbuch MS, Shepard E, Vernon-Roberts B. Morton's metatarsalgia due to intermetatarsophalangeal bursitis as an early manifestation of rheumatoid arthritis. Clin Orthop 1982; 167: 214–221.
29. Zanetti M, Strehle JK, Kundert HP, Zollinger H, Hodler J. Morton neuroma: effect of MR imaging findings on diagnostic thinking and therapeutic decisions. Radiology 1999; 213:583–588.
30. Redd RA, Peters VJ, Emery SF, et al. Morton neuroma: sonographic evaluation. Radiology 1989; 171:415–417.
31. Sobiesk GA, Wertheimer SJ, Schulz R, et al. Sonographic evaluation of interdigital neuromas. J Foot Ankle Surg 1997; 36:364–366.
32. Shapiro PP, Shapiro SL. Sonographic evaluation of interdigital neuromas. Foot Ankle Int 1995; 16:604–606.
33. Fessell DP, van Holsbeeck MT. Foot and ankle sonography. Radiol Clin North Am 1999; 37: 831–858.
34. Oliver TB, Beggs I. Ultrasound in the assessment of metatarsalgia: a surgical and histologic correlation. Clin Radiol 1998; 53:287–289.
35. Murphey MD, Smith WS, Smith SE, et al. Imaging of musculoskeletal neurogenic tumors: radiologic-pathologic correlation. RadioGraphics 1999; 19:1253–1280.
36. Read JW, Noakes JB, Kerr D, et al. Morton's metatarsalgia: sonographic findings and correlated histopathology. Foot Ankle Int 1999; 20: 153–161.
37. Zanetti M, Ledermann T, Zollinger H, et al. Efficacy of MR imaging in patients suspected of having Morton's neuroma. AJR Am J Roentgenol 1997; 168:529–532.

This article meets the criteria for 1.0 credit hour in category 1 of the AMA Physician's Recognition Award. To obtain credit, see accompanying test at http://www.rsna.org/education/rg_cme.html.